Measurements of transition probabilities in ^{52,54}Ti to probe shell evolution toward $N = 32$

A. Goldkuhle,[1,a] C. Fransen,[1] A. Blazhev,[1] M. Beckers,[1] B. Birkenbach,[1] T. Braunroth,[1] E. Clément,[2] A. Dewald,[1] J. Dudouet,[3] J. Eberth,[1] H. Hess,[1] B. Jacquot,[2] J. Jolie,[1] Y.-H. Kim,[4] A. Lemasson,[2] S. M. Lenzi,[5,6] H. J. Li,[2] J. Litzinger,[1] C. Michelagnoli,[5,6,2] C. Müller-Gatermann,[1] R. M. Perez-Vidal,[7] D. Ralet,[8,9,10] P. Reiter,[1] M. Rejmund,[2] A. Vogt,[1] N. Warr,[1] K. O. Zell,[1] N. Alahari,[2] A. Ataç,[11] D. Barrientos,[12] C. Barthe-Dejean,[2] G. Benzoni,[13] A. J. Boston,[14] H. C. Boston,[14] P. Bourgault,[2] I. Burrows,[15] J. Cacitti,[2] B. Cederwall,[11] M. Ciemala,[16] D. M. Cullen,[17] G. De France,[2] C. Domingo-Pardo,[7] F. J. Egea Canet,[5] J. L. Egido,[18] J.-L. Foucher,[2] G. Fremont,[2] A. Gadea,[7] P. Gangnant,[2] V. González,[19] J. Goupil,[2] C. Henrich,[10] C. Houarner,[2] M. Jean,[2] D. S. Judson,[14] A. Korichi,[8] W. Korten,[20] A. Lefevre,[2] L. Legeard,[2] F. Legruel,[2] S. Leoni,[13,21] J. Ljungvall,[8] A. Maj,[16] C. Maugeais,[2] L. Ménager,[2] N. Ménard,[2] R. Menegazzo,[5] D. Mengoni,[5,6] B. Million,[13] H. Munoz,[2] B. S. Nara Singh,[17] D. R. Napoli,[22] J. Nyberg,[23] M. Ozille,[2] Zs. Podolyak,[24] A. Pullia,[13,25] B. Raine,[2] F. Recchia,[5,6] J. Ropert,[2] F. Saillant,[2] M. D. Salsac,[20] E. Sanchis,[19] C. Schmitt,[2] J. Simpson,[15] C. Spitaels,[2] O. Stezowski,[3] Ch. Theisen,[20] M. Toulemonde,[26] M. Tripon,[2] J.-J. Valiente Dobón,[22] G. Voltolini,[2] and M. Zielińska[20]

[1] *Institut für Kernphysik, Universität zu Köln, 50937 Köln, Germany*
[2] *GANIL, CEA/DRF-CNRS/IN2P3, BP 55027, 14076 Caen Cedex 5, France*
[3] *Université de Lyon, CNRS/IN2P3, IPN-Lyon, F-69622 Villeurbanne, France*
[4] *Institut Laue-Langevin, BP 156, 38042 Grenoble Cedex 9, France*
[5] *INFN Sezione di Padova, I-35131 Padova, Italy*
[6] *Dipartimento di Fisica e Astronomia dell'Università di Padova, I-35131 Padova, Italy*
[7] *Instituto de Física Corpuscular, CSIC-Universidad de Valencia, E-46071 Valencia, Spain*
[8] *Centre de Spectrométrie Nucléaire et de Spectrométrie de Masse - CSNSM, CNRS/IN2P3 and Université Paris-Sud, F-91405 Orsay Campus, France*
[9] *GSI, Helmholtzzentrum für Schwerionenforschung GmbH, 64291 Darmstadt, Germany*
[10] *Institut für Kernphysik, Technische Universität Darmstadt, 64289 Darmstadt, Germany*
[11] *Department of Physics, Royal Institute of Technology, SE-10691 Stockholm, Sweden*
[12] *CERN, CH-1211 Geneva 23, Switzerland*
[13] *INFN Sezione di Milano, I-20133 Milano, Italy*
[14] *Oliver Lodge Laboratory, The University of Liverpool, Liverpool, L69 7ZE, UK*
[15] *STFC Daresbury Laboratory, Daresbury, Warrington WA4 4AD, UK*
[16] *The Henryk Niewodniczański Institute of Nuclear Physics, Polish Academy of Sciences, ul. Radzikowskiego 152, 31-342 Kraków, Poland*
[17] *Nuclear Physics Group, Schuster Laboratory, University of Manchester, Manchester, UK*
[18] *Departamento de Física Teórica, Universidad Autónoma de Madrid, 28049 Madrid, Spain*
[19] *Departamento de Ingeniería Electrónica, Universitat de Valencia, Burjassot, Valencia, Spain*
[20] *Irfu, CEA, Université Paris-Saclay, F-91191 Gif-sur-Yvette, France*
[21] *Dipartimento di Fisica, Università di Milano, I-20133 Milano, Italy*
[22] *Laboratori Nazionali di Legnaro, INFN, I-35020 Legnaro, Italy*
[23] *Department of Physics and Astronomy, Uppsala University, SE-75120 Uppsala, Sweden*
[24] *Department of Physics, University of Surrey, Guildford, GU2 7XH, UK*
[25] *University of Milano, Department of Physics, I-20133 Milano, Italy*
[26] *CIMAP-GANIL (CEA-CNRS-ENSICAEN-Université de Caen), BP 5133, 14070 Caen, France*

(Dated: August 2, 2019)

Transition probabilities from lifetimes of excited states in neutron-rich nuclei ^{52,54}Ti, produced in a multinucleon-transfer reaction, were measured employing the recoil distance Doppler-shift (RDDS) method. The experiment was performed at the Grand Accélérateur National d'Ions Lourds (GANIL) facility by using the Advanced Gamma Tracking Array (AGATA) for the γ-ray detection and the Cologne plunger device for deep inelastic reactions, coupled to the large-acceptance variable mode spectrometer (VAMOS++) for an event-by-event particle identification. The aim was the investigation of the evolution of the shell structure in the vicinity of the $N = 32$ subshell. Level lifetimes and lifetime limits of the 2_1^+ to 8_1^+ states of the yrast bands in ^{52,54}Ti are determined. The obtained transition probabilities are compared to shell-model calculations based on established fp shell interactions.

PACS numbers:

I. INTRODUCTION

Understanding the evolution of shell structure towards the drip lines is one of the driving forces for many theoret-

[a] Corresponding author: agoldkuhle@ikp.uni-koeln.de

ical and experimental effort, as investigations have shown that the shell structure often changes drastically as a result of the rearrangement of single particle levels in exotic nuclear regions [1]. In this context, the $N = 40$ island of inversion represents a rich testing ground. For example, an increasing collectivity was identified both from excitation energies and transition strengths in neutron rich $^{58-66}$Cr [2–5] and $^{62-70}$Fe [5–8] close to the $Z = 28$ shell closure. The data resulted in a conclusive description of these nuclei with respect to the observed high collectivity with modern shell-model calculations [2, 6].

Studies of neutron rich Ti isotopes are also essential for an understanding of the shell structure in the Ti-Cr-Fe region beyond $N = 28$ towards $Z = 20$. Existing $B(E2, 2_1^+ \rightarrow 0_{gs}^+)$ values in ^{52}Ca [9], ^{54}Ti [10], ^{56}Cr [11, 12], ^{58}Fe [13] and ^{60}Ni [14], pictured in a shell-model framework as a completely filled valence $\nu 2p_{3/2}$ orbital, suggest a phase transition from predominant collective structures in ^{58}Fe that evolves toward a neutron subshell closure along the isotonic chain with decreasing proton number, i.e. from ^{56}Cr$\rightarrow$ ^{54}Ti$\rightarrow$ ^{52}Ca. This is supported by an increased staggering of 2_1^+ excitation energies for decreasing proton number as shown in Fig. 1. At the neutron shell closure $N = 28$, all depicted isotopes show a local rise in the 2_1^+ state energy but at $N = 32$ a different behavior is observed: only ^{52}Ca, ^{54}Ti and ^{56}Cr exhibit a local increase in the 2_1^+ state energy. The corresponding $B(E2; 2_1^+ \rightarrow 0_{gs}^+)$ values suggest a weak and very localized subshell closure at $N = 32$ [9] for Ca-Ti-Cr which collapses toward Fe and Ni. This behavior was investigated in several recent experiments on ^{52,54,56}Ti and ^{58}Cr using deep inelastic reactions [15, 16], β-decay [17, 18] as well as Coulomb excitation at intermediate energies [10].

A possible explanation could be an effect similar to that for $N = 40$ isotones described in works of T. Otsuka *et al.* [19–21] proposing the monopole component of the proton-neutron tensor force as one of the driving forces behind shell evolution at $N = 40$. This ensures that the $N = 40$ gap is reduced by removing protons from the $\pi 1f_{7/2}$ subshell. For nuclei close to $N = 32$ a comparable effect could result in an inverse order of the $\nu 1f_{5/2}$ and $\nu 2p_{1/2}$ orbitals and is assumed to contribute to the evolution of a shell gap at $N = 32$, i.e. between $\nu 2p_{3/2}$ and $(\nu 2p_{1/2}, \nu 1f_{5/2})$ orbitals with decreasing proton number from $Z = 28$ to $Z = 20$.

For a better understanding of the actual situation data on $E2$ transition strengths between higher spin states in ^{54}Ti are essential, which are not available to date. Furthermore, in the neighboring nucleus ^{52}Ti the shell-model predictions do not agree with the transition strengths between the lowest yrast states deduced in Ref. [22] showing an opposite behavior compared to the neighbors ^{50,54}Ti [22]. So far, no successful description of the shell model could be found in ^{52}Ti. These motivate a new detailed investigation of ^{52}Ti and a reinvestigation of ^{54}Ti in order to obtain a comprehensive picture of the evolving shell structure with regard to the appearance of a $N = 32$ subshell closure for $Z < 26$.

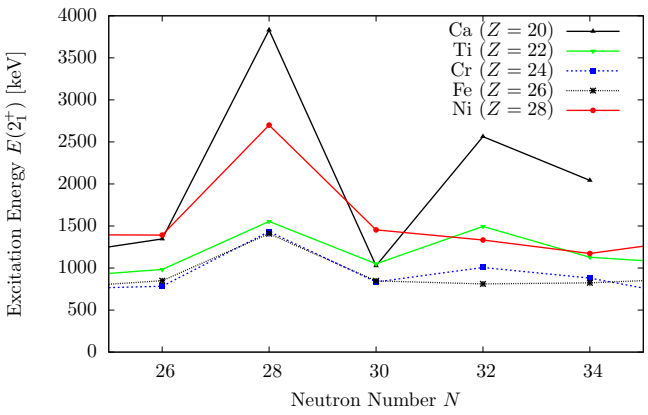

Figure 1. (Color online) Evolution of experimental excitation energies $E(2_1^+)$ in neutron rich even-even Ca-Ni nuclei with $20 \leq Z \leq 28$ and $26 \leq N \leq 34$.

In this work, the evolution of the shell structure in ^{52,54}Ti is studied by measuring the lifetimes of the lowest excited yrast states ($2_1^+, 4_1^+, 6_1^+$ and 8_1^+) employing the recoil distance Doppler-shift (RDDS) method [23]. The deduced $E2$ transition strengths will be discussed in the framework of current shell-model calculations.

II. EXPERIMENTAL SETUP

The RDDS experiment on ^{52,54}Ti was performed at the Grand Accélérateur National d'Ions Lourds (GANIL) in Caen, France using the Cologne plunger for deep inelastic reactions, as described in Ref. [23]. The ^{52,54}Ti nuclei were produced by a multinucleon-transfer reaction induced by a ^{238}U beam at an energy of $E(^{238}\text{U}) = 1608.9\,\text{MeV}$ ($= 6.76\,\text{MeV/u}$) applied to a ^{50}Ti target. The thickness of the target amounted to $1.5\,\text{mg/cm}^2$, on which a natural copper fronting with a thickness of $0.4\,\text{mg/cm}^2$ was evaporated. The plunger device including target and degrader foils was placed at an angle of 45° with respect to the incoming beam which is close to the grazing angle of the multinucleon transfer reactions of interest. Target and degrader foils are, therefore, mounted orthogonal to the entry axis of the magnetic spectrometer VAMOS++. Thus the ^{50}Ti target layer had an effective thickness of $2.1\,\text{mg/cm}^2$ which lead to a ^{238}U beam energy of $6.16\,\text{MeV/u}$ in the middle of the ^{50}Ti layer also taking into account the energy loss in the Cu fronting layer with an effective thickness of $0.57\,\text{mg/cm}^2$. A $^{\text{nat}}$Mg degrader foil with a thickness of $3.2\,\text{mg/cm}^2$ was placed downstream from the target, so that target-like recoils were slowed down before entering the VAMOS++ magnetic spectrometer [24–26]. The latter was used for the event-by-event particle identification. During the experiment, VAMOS++ consisted of

two quadrupoles, a dipole magnet and the focal plane detectors. A schematic drawing of the experimental setup is shown in Fig. 1 in Ref. [27]. The focal plane detection system is used to identify the mass (A), charge (Q) and atomic number (Z) of the target reaction products consisted of a multi-wire proportional counter (MWPC), four drift chambers and a segmented ionization chamber. The Dual Position-Sensitive Multi-Wire Proportional Counter (DPS-MWPC) [26] placed at the entrance of the spectrometer provided the start signal for the time-of-flight (TOF) and the position (x, y) of the reaction products. Together with the MWPC in the focal plane they give the TOF and indicated the direction of the ions for Doppler-correction. The drift chambers, which also detected the position (x, y) as well as the emission angles (θ, ϕ) of the recoiling reaction products, are used together with the DPS-MWPC to determine the trajectory of the ions after the dipole magnet. Finally ionization chambers are employed for measuring the total energy E and energy loss ΔE of the ions at the focal plane. In this experiment the magnetic rigidity of VAMOS++ was set to $B\rho = 0.975\,\mathrm{Tm}$ for the detection of the nuclei of interest in the focal plane detectors.

Prompt γ rays were detected by the Advanced Gamma Tracking Array (AGATA) [28, 29]. At the time of this experiment it consisted of 29 36-fold segmented capsules in 10 cryostats placed at a radial distance of 23.5 cm with respect to the target center and covered angles from 120° to 175° with respect to the optical axis of the spectrometer. Using the velocity vector as reconstructed by VAMOS++, and together with the position of the first interaction point in AGATA, the observed γ-rays were Doppler-corrected using on an event-by-event basis using the angle between the scattered particle and the direction of γ rays detected in AGATA. The particle velocity after passing the degrader foil is used for the Doppler correction. Then the slow component, i.e. emission after the degrader, occurs at the nominal γ-ray energy whereas the fast component is shifted toward lower energies, as AGATA was located at backwards angles.

Data were taken at six different nominal target-to-degrader distances between 70 µm and 1000 µm for about 24 h per distance, which results in a sensitivity to lifetimes ranging from few ps to about 400 ps. During the experiment, despite the low beam current of 0.1 pnA, beam-induced changes of the ^{50}Ti target occurred that will be described in the following. A single-layer self-supporting ^{50}Ti target with a thickness of $1.5\,\mathrm{mg/cm^2}$ was used at first. This target got wrinkle-like structures with an amplitude of about 100 µm directly after being exposed to the 6.76 MeV/u ^{238}U beam with a beam current of 0.1 pnA. To improve heat conductivity this target was replaced with the aforementioned $1.5\,\mathrm{mg/cm^2}$ ^{50}Ti target with an additional $0.4\,\mathrm{mg/cm^2}$ copper layer that as evaporated onto the ^{50}Ti. This was done even though estimates of the beam spot temperature from the momentum transfer of the beam yielded no significant thermal load. The copper layer was facing the beam. This target got similar damages after being exposed to the beam (see Fig. 2). Nevertheless, as no other alternative was available the ^{50}Ti target with the additional copper layer had to be used for the experiment presented in this work in spite of the structural changes.

After a careful analysis in retrospect of the experiment it turned out that the observed degradation of the target can be explained as resulting from the sensitivity of Ti to the electronic stopping of heavy ions (see Ref. [30]). This effect leads to a drastic increment of the lattice temperature of Ti induced by the irradiation by the highly energetic ^{238}U ions (so-called thermal spikes) and thus to structural damages of the Ti target foil [30]. Ti is very sensitive to this effect due to its large Debye temperature on the one hand and its low thermal conductivity on the other hand. This observation can be reproduced within the thermal spike model (see, e.g., Ref. [31]). Since Magnesium has a much lower Debye temperature and a higher thermal conductivity, no effects were observed with respect to the degrader.

For this reason a "simple" and precise determination of the distances between the plunger target and the degrader was not possible. Instead, average absolute distances for each distance setting need to be specified as the structural changes take place as long as the target is exposed to the ^{238}U beam. These distances are denoted as "effective" distances in the following and can be extracted from γ-ray spectra related to nuclear states whose lifetimes are known with high precision. A strongly populated reaction channel led to ^{46}Ti (see Fig. 3 for the corresponding spectrum). A high-precision RDDS $\gamma\gamma$ coincidence experiment on ^{46}Ti was performed only recently and results were published in Ref. [32].

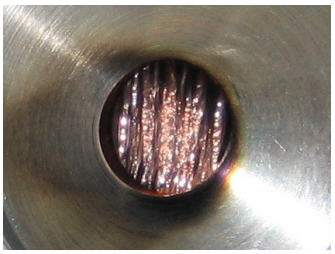

Figure 2. (Color online) Beam induced changes of the ^{50}Ti plunger target: The originally stretched target foil is severely damaged. Shown is the side of the target that was facing the beam with the copper layer.

For the determination of effective distances γ-ray spectra for ^{46}Ti were created through a versatile Geant4-based Monte-Carlo simulation tool [33] using a precise reproduction of the experimental geometry including the target chamber and the AGATA detectors. For the distance determination distance assumptions are fed into the simulation tool-kit and their values are varied in discrete steps. For each comparison between the simulated and the experimental spectrum a χ^2 was calculated according to the following modified version of the least-

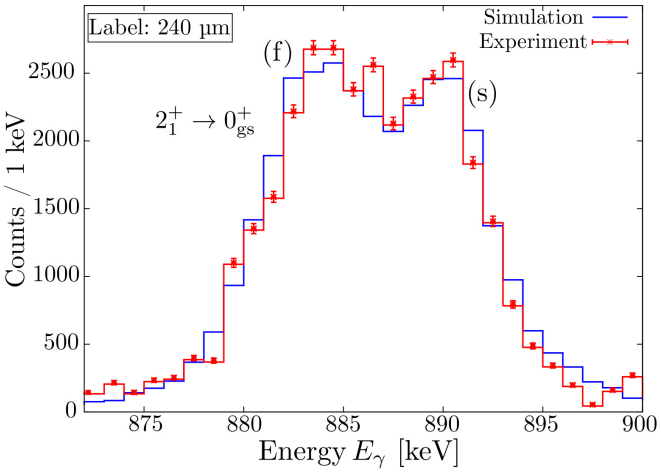

Figure 3. (Color online) Experimental (red) and simulated (blue) γ-ray energy spectra in ^{46}Ti at an effective target-to-degrader distance of 277 µm Doppler-corrected for the degraded component. The fast (f) and slow (s) components are additionally labeled. See text for details.

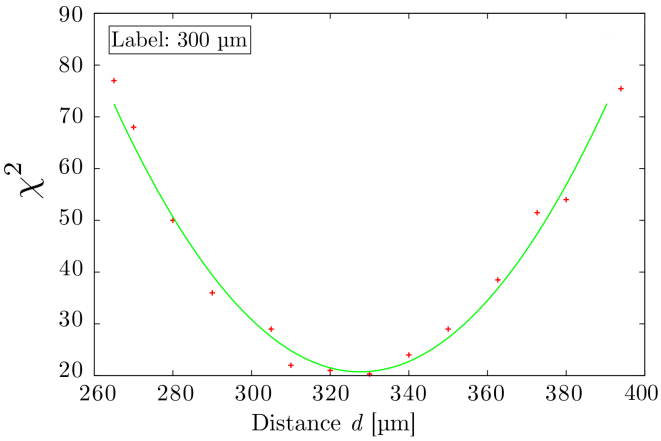

Figure 4. (Color online) Determination of the mean distance using the standard χ^2 method. The errors of the χ^2 method are deduced from lifetimes with $\chi^2_{\text{min}} + 1$. See text for details.

squares method using

$$\chi^2 = \sum_i \left(\frac{I_{\text{exp}}(i) - I_{\text{sim}}(i)}{I_{\text{exp}}(i)} \right)^2$$

where $I_{\text{exp}}(I_{\text{sim}})$ is the intensity of the experimental (simulated) spectrum in bin i. The chosen range was restricted to both fast and slow components of the considered transition. An exemplary result of this approach with the standard χ^2 method is depicted in Fig. 4. The statistical uncertainty is extracted from distance values at $\chi^2_{\text{min}} + 1$. For illustration, Fig. 3 shows a representative comparison of the experimental spectra showing the $2_1^+ \rightarrow 0_{gs}^+$ transition in ^{46}Ti at a nominal distance of 240 µm as well as the best-fitting simulation assuming a separation following the given approach. A similar picture can be seen with the other distances. Table I shows the effective distances d resulting from the individual ^{46}Ti simulations.

Table I. Results of the "effective" distances d resulting from simulations and the nominal distances d_{exp} (i.e. relative to electrical contact before the experiment) during the experiment.

d_{exp} [µm]	d [µm]
70	102(8)
150	198(9)
180	200(6)
240	277(10)
300	328(9)

The velocities of the recoils were determined as follows: the velocity of the isotopes recoiling after the degrader was measured directly by VAMOS++, whereas the velocity between target and degrader was deduced from the experimental Doppler shift between the two components of the transitions. The mean recoil velocity behind the target (degrader) is $\beta_T = 12.70(21)\,\%$ ($\beta_D = 11.68(23)\%$) of the speed of light.

III. DATA ANALYSIS AND RESULTS

Using the VAMOS++ spectrometer, the target-like reaction products were identified by their mass, charge and atomic number. Nuclei with the same atomic number Z were identified by their energy loss ΔE as a function of the total kinetic energy E, as shown in Fig. 5. The reconstruction of the trajectories gives information about the magnetic rigidity $B\rho$ and the angle at the target position. The mass-over-charge (A/Q) ratio and the mass A are determined from the TOF, the path through the spectrometer, and the magnetic rigidity. The mass resolution for the isotopic chains, shown in Fig. 5, was $\frac{\Delta M}{M} \approx 1.4\,\%$, so that an unambiguous identification of the reaction residues in the mass region around $A = 50$ was possible.

Depending on whether the γ decay of an excited nuclear state occurred in flight between target and degrader or after slowing down in the degrader, the γ rays exhibited different Doppler shifts. Figure 6 shows the resulting γ-ray spectra after Doppler correction for the slow component detected with AGATA in coincidence with the signal of ^{54}Ti and ^{52}Ti, summed over all six distances. It can be clearly seen that the statistics for ^{52}Ti is ~ 13 times higher than in ^{54}Ti. The higher energy (slow) component corresponds to the γ rays emitted after the degrader, while the lower energy (fast) component corresponds to γ rays emitted before traversing the degrader, when observed under backward angles.

The clearly visible development of the intensities of the fast and slow components with the distance d in

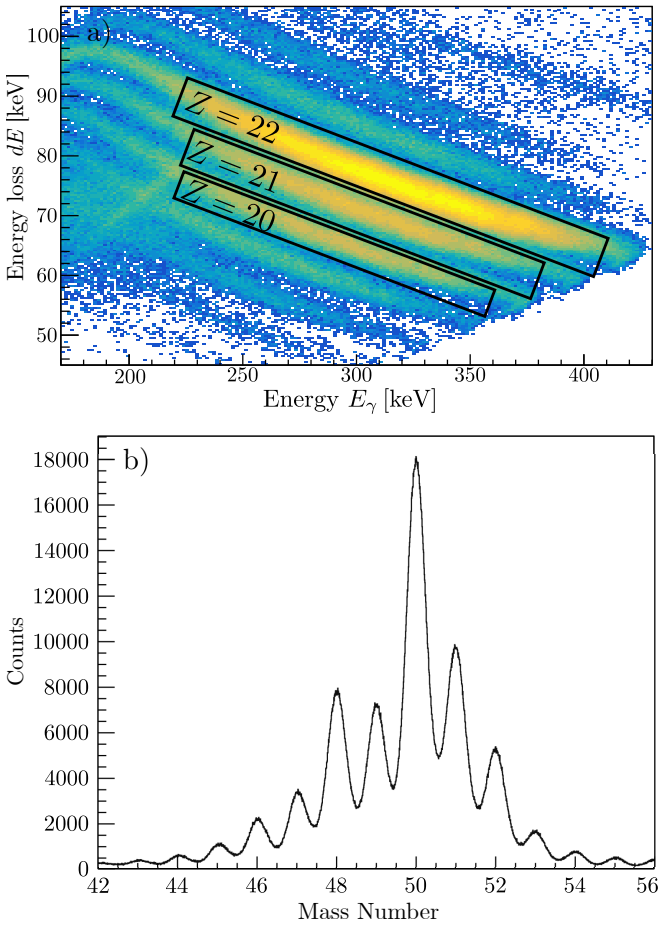

Figure 5. (Color online) a) Energy loss of the target-like reaction products in VAMOS++ as a function of total detected energy. The separation of the isotopes of titanium ($Z = 22$), scandium ($Z = 21$) and calcium ($Z = 20$) is marked schematically with black rectangles. Graphic b) shows the mass resolution for the titanium isotopic chain.

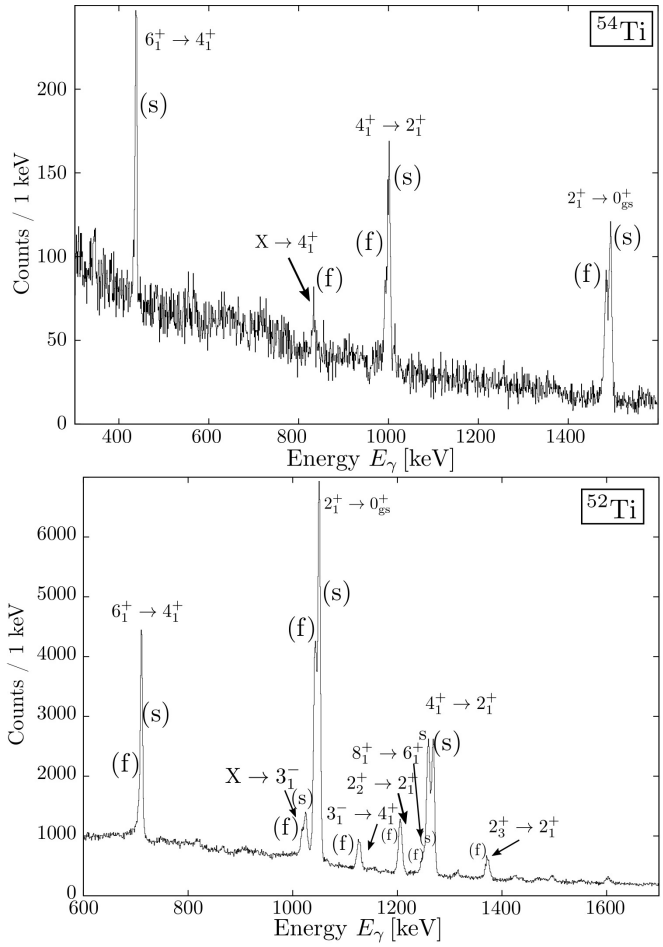

Figure 6. Gamma-ray spectra in coincidence with ions identified as ^{54}Ti (*top*) and ^{52}Ti (*bottom*), summed over all six distances. In this energy range four (eight) γ-ray decays are visible in ^{54}Ti (^{52}Ti). The fast (f) and slow (s) components are additionally labeled.

the Doppler-corrected energy spectra for the $2^+_1 \rightarrow 0^+_{gs}$ transition of ^{54}Ti at three different distances is shown in Fig. 7. During the fitting procedure the peak positions and widths were fixed. The latter were determined by calibrating the line width using the γ-ray spectra of ^{50,52,53}Ti with a significantly larger γ-ray yield than of ^{54}Ti. Due to the relatively small difference in the velocity of $\Delta v = 0.0102\,c$ the components of the fast and slow components of the γ-ray lines are not well separated from each other. A thicker degrader would have resulted in a better separation of the Doppler-shifted components. However, such could not be used as the higher scattering on the degrader would have caused an overload of the start MWPC at the entrance of VAMOS++.

Lifetimes of excited states of ^{52,54}Ti were extracted from γ-ray intensities for each distance in the sensitive range (see Eq. (20) in Ref. [23]) using the differential decay curve method (DDCM) presented in detail in Ref. [34]. Therefore, the obtained value of the lifetime should not depend on the target-to-degrader distances at which it has been determined, so that a constant line of τ values is expected by plotting versus the distances. In ^{54}Ti it was possible to identify five transitions that are clearly visible after Doppler correction for the slow component: $2^+_1 \rightarrow 0^+_{gs}$ (1495 keV), $4^+_1 \rightarrow 2^+_1$ (1002 keV), $6^+_1 \rightarrow 4^+_1$ (439 keV), $8^+_1 \rightarrow 6^+_1$ (2523 keV) and a transition from a state with unknown spin and parity I^π to the 4^+_1 at 840 keV. Only for the $2^+_1 \rightarrow 0^+_{gs}$ and $4^+_1 \rightarrow 2^+_1$ transitions both components were visible at all distances. For the $6^+_1 \rightarrow 4^+_1$ transition at 439 keV only the slow component was visible at all distances, so that only a lower limit of the 6^+ lifetime was determined. In contrast, for the $8^+_1 \rightarrow 6^+_1$ transition at 2523 keV only the fast component was visible at all distances, so that an upper limit of the 8^+_1 lifetime was measured. In ^{52}Ti it was possible to identify ten transitions: $2^+_1 \rightarrow 0^+_{gs}$ (1050 keV), $4^+_1 \rightarrow 2^+_1$ (1268 keV), $6^+_1 \rightarrow 4^+_1$ (711 keV), $8^+_1 \rightarrow 6^+_1$ (1258 keV), $2^+_2 \rightarrow 2^+_1$ (1214 keV), $2^+_3 \rightarrow 2^+_1$ (1382 keV), $3^-_1 \rightarrow 4^+_1$ (1135 keV), $(10^+_1) \rightarrow 8^+_1$ (2406 keV), $10^+_2 \rightarrow 8^+_1$ (3232 keV), and a transition from a state with unknown

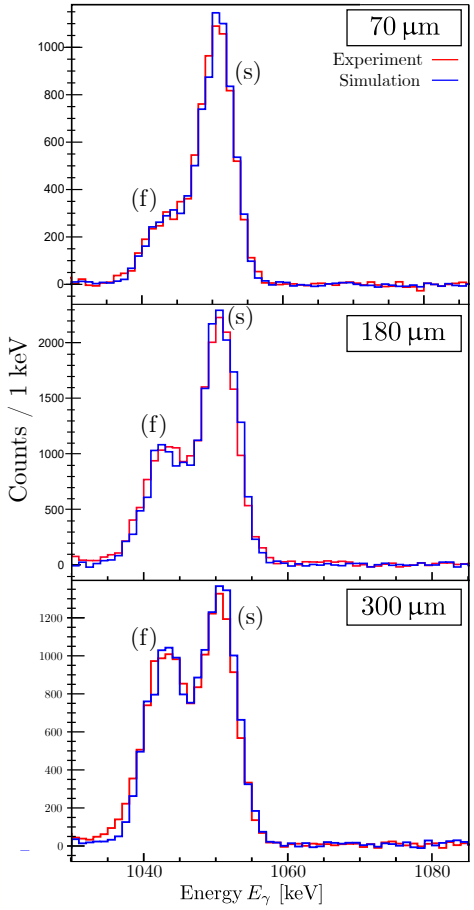

Figure 7. Simulated (blue) and experimental (red) γ-ray energy spectra of the $2_1^+ \rightarrow 0_{gs}^+$ transition at 1495 keV in ^{54}Ti at three target-to-degrader distances at backward angles. The development of intensity ratios of the fast (f) and slow (s) components with increasing distances is clearly visible.

spin and parity I^π to the 3_1^- at 1025 keV. For the lifetime determination of the $2_1^+, 4_1^+, 6_1^+$ and 8_1^+ states a feeding correction was carried out by subtracting the efficiency corrected and normalized intensities of the slow component of a direct feeder from the intensity of the slow component of the state to be analyzed. All contributions from states outside the yrast band have been neglected due to non-existing slow components, which means that these states are characterized by a rather small (prompt) level lifetime. It should be mentioned that the fast component of the $4_1^+ \rightarrow 2_1^+$ transition is equal in energy to the slow component of the $8_1^+ \rightarrow 6_1^+$ transition. This was taken into account in the analysis by calculating the respective proportions accordingly. For this purpose, an intensity function depending on the spin was first established by determining the intensities of the fast and slow components of the $2_1^+ \rightarrow 0_{gs}^+$, $6_1^+ \rightarrow 4_1^+$ and $10_2^+ \rightarrow 8_1^+$ transitions in ^{52}Ti in the spectrum summed up over all distances. This intensity function was compared to that function of ^{48}Ti and is possible due to similar level schemes. Using the intensity function, the summed intensities $(I_{f+s}(I_1^+ \rightarrow (I-2)_1^+))$ of the fast and slow components of the $4_1^+ \rightarrow 2_1^+$ and $8_1^+ \rightarrow 6_1^+$ transitions in ^{52}Ti were calculated. Then the intensities of the $2_1^+ \rightarrow 0_{gs}^+$ transitions were determined for each distance and the unknown intensities of the $4_1^+ \rightarrow 2_1^+$ and $8_1^+ \rightarrow 6_1^+$ were calculated according to $I_{f+s,dist}(I_1^+ \rightarrow (I-2)_1^+) = \alpha_i \cdot I_{f+s}(2_1^+ \rightarrow 0_{gs}^+)$ with $\alpha_i = \frac{I_{f+s}(I_1^+ \rightarrow (I-2)_1^+)}{I_{f+s}(2_1^+ \rightarrow 0_{gs}^+)}$.

The relevant plots for the lifetime analysis for the decay of the 2_1^+ and 4_1^+ states in ^{54}Ti (^{52}Ti) are shown in Fig. 8 (Fig. 9). The related fits of the intensities of the two components were done with the code NAPATAU [35]. The weighted average lifetime is taken of the points inside the region of sensitivity, e.g. where the slope of the decay curve is at the half of the maximum value. The weighted averages of the mean lifetimes in ^{52,54}Ti are summarized along with the $E2$ transition strengths in Table II. The statistical uncertainty of each lifetime value is dominated by the distribution of the individual τ-values. The uncertainty of the recoil velocity and the uncertainty of the relative target-to-degrader distances define the systematic errors of the lifetime. The final experimental error of the lifetime includes the root sum squared of the statistical and the systematic uncertainties.

In addition, the lifetimes determined according to DDCM were verified with the Geant4-based Monte-Carlo tool. Fig. 7 shows a comparison between the experimental and simulated γ-ray spectra for ^{52}Ti at three different distances.

The lifetime $\tau(2_1^+) = 1.3(5)$ ps of the 2_1^+ state in ^{54}Ti determined in this work corresponds to a reduced transition probability of $B(E2; 2_1^+ \rightarrow 0_{gs}^+) = 84^{+53}_{-23}\, e^2\text{fm}^4$ and agrees with the adopted lifetime $\tau(2_1^+) = 1.53(27)$ ps with corresponding $B(E2; 2_1^+ \rightarrow 0_{gs}^+) = 72^{+15}_{-11}\, e^2\text{fm}^4$ [10] within their error limits.

In ^{52}Ti there is a considerable discrepancy between the new $B(E2; I_1^+ \rightarrow (I-2)_1^+)$ values in this work for $I = 2, 4, 6$ and the previously measured $B(E2)$ values by Speidel *et al.* [22] (cf. Fig. 12). The lifetime values of the 2_1^+ and 4_1^+ states from Ref. [22] and this measurement differ by a factor of ~ 2.

IV. DISCUSSION

A. Systematics

The results of this work yield new insights in the shell evolution for neutron-rich Ti-Cr-Fe isotopes. Figure 10 illustrates the systematics of excitation energies and the evolution of $B(E2; 2_1^+ \rightarrow 0_{gs}^+)$ values for even-even nuclei with $20 \leq Z \leq 28$ and $26 \leq N \leq 34$. While the rest of the values correspond to the adopted ones, the $B(E2; 2_1^+ \rightarrow 0_{gs}^+)$ value for ^{52}Ti is the one determined in this work and for ^{54}Ti the one from Ref. [10] as it is consistent with our new value but has a smaller uncertainty.

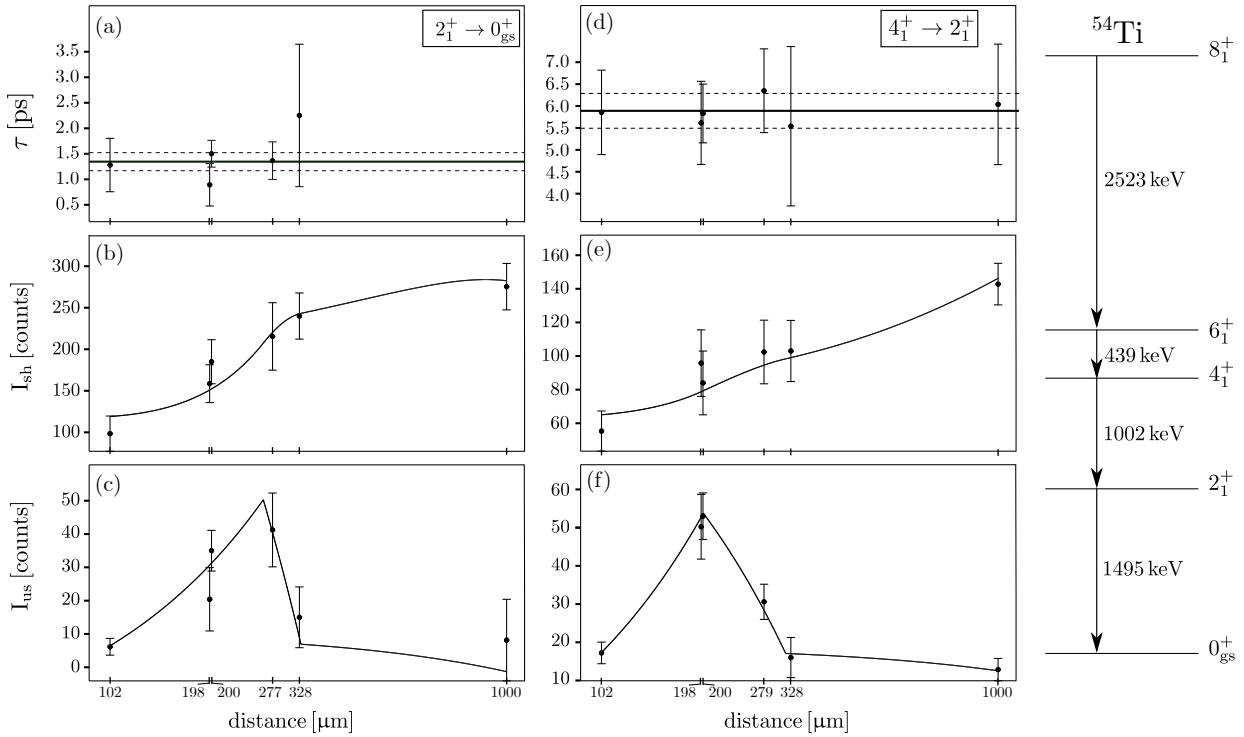

Figure 8. Tau-curves (a),(d) of the 2_1^+ (*left*) and 4_1^+ (*middle*) states in ^{54}Ti. Black solid lines in (a),(d) represent the weighted mean value of the lifetime; dashed lines mark the statistical uncertainty. In addition, the intensities of the fast (b),(e) and slow (c),(f) components are shown, where the latter are corrected for delayed observed feeding. The polynomial fit function to the given intensities is presented in solid black in (b),(e) and (c),(f). Note the logarithmic distance scale. *Right:* Partial level scheme with the relevant γ transitions of the yrast band observed in the γ-ray spectrum of ^{54}Ti.

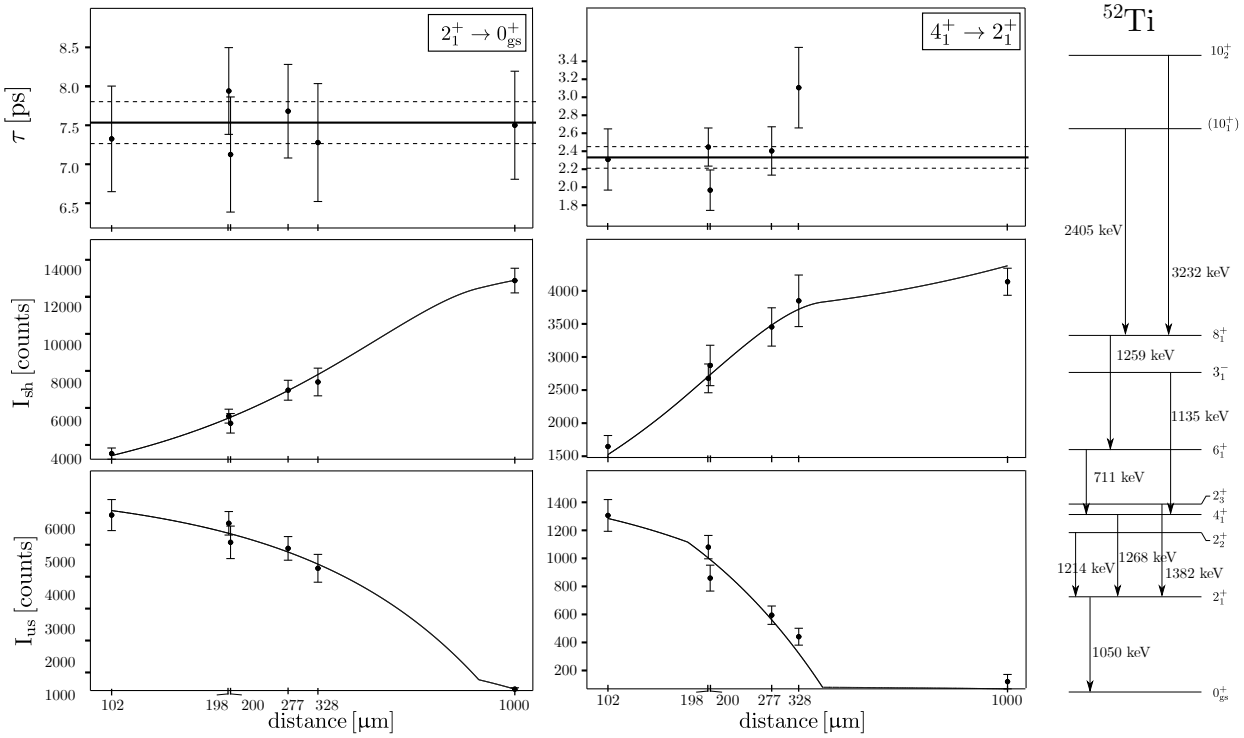

Figure 9. Similar diagram as presented in Fig. 8 for the 2_1^+ (*left*) and 4_1^+ (*middle*) states in ^{52}Ti. *Right:* Level scheme of the relevant γ transitions observed in the γ-ray spectrum of ^{52}Ti.

411 At the neutron shell closure $N = 28$, all depicted iso- 412 topes are characterized locally by high excitation energies

Table II. Lifetime values for the first four yrast states in ^{52,54}Ti from the present experiment are compared to previous experimental values taken from Refs. [10, 22]. The corresponding experimental $B(E2; I_1^+ \rightarrow (I-2)_1^+)$ values are included.

Nucleus	^{52}Ti				^{54}Ti			
	Lifetime [ps]		$B(E2)$ [e^2fm^4]		Lifetime [ps]		$B(E2)$ [e^2fm^4]	
I_1^+	Present	Previous [22]	Present	Previous [22]	Present [10]	Previous	Present	Previous [10]
2_1^+	7.5(4)	5.19(20)	86^{+5}_{-4}	124^{+5}_{-5}	1.3(5)	1.53(27)	84^{+53}_{-23}	72^{+15}_{-11}
4_1^+	2.3(3)	4.76(58)	109^{+16}_{-13}	53^{+7}_{-6}	5.9(9)	-	139^{+25}_{-18}	-
6_1^+	45.0(31)	36.07(577)	100^{+7}_{-6}	125^{+24}_{-17}	≥ 380	-	≤ 132	-
8_1^+	29.4(21)	-	8.8^{+1}_{-1}	-	≤ 1.4	-	≥ 5.7	-

$E(2_1^+)$ and relatively small $B(E2; 2_1^+ \rightarrow 0_{gs}^+)$ values (see Fig. 10). At $N = 30$ all represented isotones show a reduction of the 2_1^+ energies, but while the $B(E2; 2_1^+ \rightarrow 0_{gs}^+)$ values in ^{54}Cr, ^{56}Fe and ^{58}Ni ($24 \leq Z \leq 28$) exhibit a clear rise, the $B(E2)$ in ^{50}Ca decreases. The present $B(E2; 2_1^+ \rightarrow 0_{gs}^+)$ value in ^{52}Ti indicates only a shallow increase compared to the neighboring values and fits nicely into the isotonic evolution.

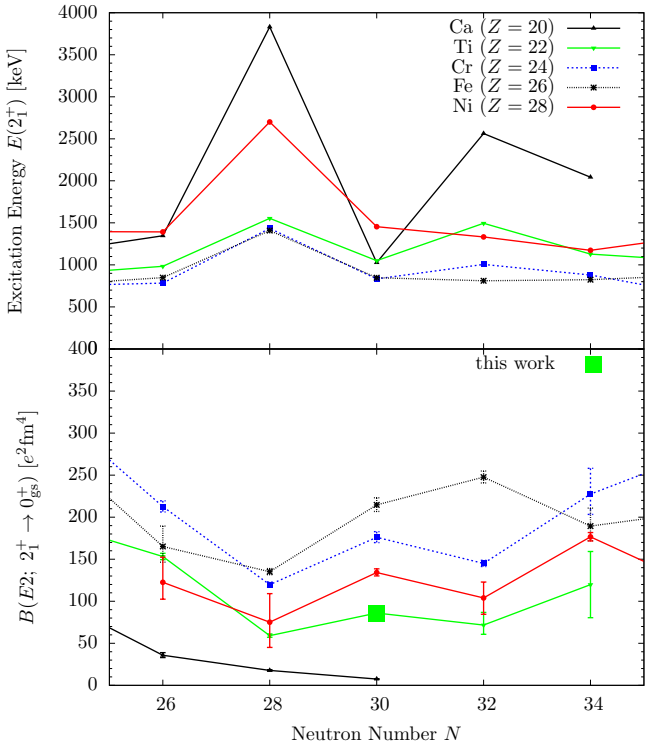

Figure 10. (Color online) Systematics of excitation energies for the 2_1^+ state (*top*) and the evolution of the $B(E2; 2_1^+ \rightarrow 0_{gs}^+)$ (*bottom*) values in even-even nuclei with $20 \leq Z \leq 28$ and $26 \leq N \leq 34$ including the result for ^{52}Ti of the present work. For ^{54}Ti the result from Ref. [10] is shown due to its smaller uncertainty.

Increasing the neutron number by two and four, the behavior of the 2_1^+ energies of Ca isotopes at $N = 32, 34$ is attributed to local $\nu 2p_{3/2}$ and $\nu 2p_{1/2}$ subshell closures as discussed in Refs. [9, 19]. We shortly remind that the relevant neutron orbitals above $N = 28$ are $\nu 2p_{3/2}$, $\nu 1f_{5/2}$ and $\nu 2p_{1/2}$. In most of the known nuclei, in the vicinity of stability, the $\nu 1f_{5/2}$ orbital is energetically close to $\nu 2p_{3/2}$, and thus no $N = 32$ shell closure is observed [10, 36]. Starting from $^{60}_{28}$Ni$_{32}$ with decreasing number of protons in the $\pi 1f_{7/2}$ orbital, i.e. from nickel to calcium, the $\nu 1f_{5/2}$ orbital becomes less bound, and at $^{52}_{20}$Ca$_{32}$ the $\nu 1f_{5/2}$ and $\nu 2p_{1/2}$ orbitals are inverted [9, 19]. The raising of the $\nu 1f_{5/2}$ orbital produces a gap between the lower-lying $\nu 2p_{3/2}$ and higher-lying $\nu 1f_{5/2}$ and $\nu 2p_{1/2}$ orbitals which leads to the local $N = 32$ subshell closure and the higher 2_1^+ energy in ^{52}Ca [9]. Thus, the phase transition from predominant collective structures in ^{60}Ni toward a neutron subshell closure at ^{52}Ca, can be attributed to the weakening of the attractive proton-neutron interaction between the $\pi 1f_{7/2}$ and $\nu 1f_{5/2}$ orbitals for decreasing number of protons in the $\pi 1f_{7/2}$ orbital [9, 19].

Figure 10 shows that in the Ti isotopes a similar peaking of 2_1^+ energy at $N = 32$ as for the Ca isotopes is observed, although with a reduced amplitude, while for Cr this effect flattens and for Fe and Ni completely disappears. This speaks for the existence of a reduced $N = 32$ subshell close also in the Ti isotopes, which has recently been confirmed also in mass measurements [36]. While the systematics of Ti $B(E2; 2_1^+ \rightarrow 0_{gs}^+)$ values from earlier experiments showed a staggering anti-correlated with the subshell closures at $N = 28$ and $N = 32$, the revised systematics of $B(E2; 2_1^+ \rightarrow 0_{gs}^+)$ values in $^{50-54}$Ti presented here, could be understood as being in contradiction to the idea of $N = 32$ subshell closure in Ti. This seemingly contradictory behavior of $E(2_1^+)$ and $B(E2; 2_1^+ \rightarrow 0_{gs}^+)$ values can be understood by addressing the nuclear structure of the lowest yrast states and the origin of $E2$ strengths in the framework of the nuclear shell model.

B. Comparison with Shell-Model Calculations

In this work, shell-model calculations were performed with the code NuShellX@MSU [37] using the interactions KB3G [38], GXPF1A [39] and GXPF1B [40]. The model space comprises the full pf main shell, coupled to a $^{40}_{20}$Ca core. Effective charges $e_\pi = 1.31\,e$ and $e_\nu = 0.46\,e$ were used for protons and neutrons, respectively, for all interactions [41]. The choice of the neutron effective charge is justified for the neighboring isotopes with $N > 28$ [42], while the microscopically justified proton effective charge [41], has an intermediate value between the standard isoscalar $e_\pi = 1.5\,e$ value and the value of $e_\pi = 1.15\,e$, which is suggested to be more adequate for the $\pi 1f_{7/2}$ orbital and especially the $N = Z$ region [43].

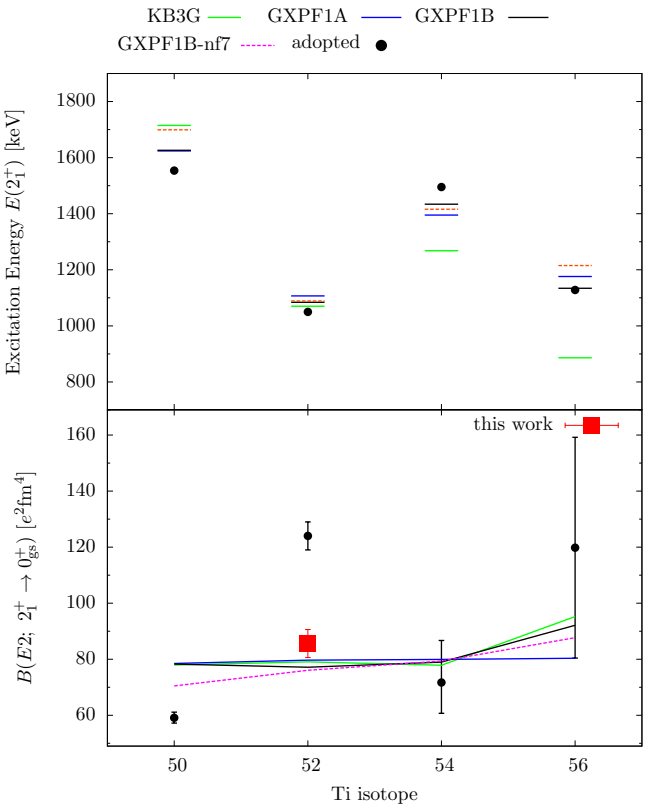

Figure 11. (Color online) Comparison of 2_1^+ excitation energies (*top*) and $B(E2; 2_1^+ \to 0_{gs}^+)$ transition strengths (*bottom*) with the results of shell-model calculations using the KB3G, GXPF1A, GXPF1B and GXPF1B-nf7 interactions for $^{50-56}$Ti.

Figure 11 shows a comparison of experimental and shell-model systematics of the 2_1^+ energies and the $B(E2; 2_1^+ \to 0_{gs}^+)$ values for $^{50-56}$Ti. The excitation energies are explicitly listed in Table III. All used interactions describe the experimental excitation energies well (see Table III).

As seen in Fig. 11 the previously adopted values produced a staggering in the $B(E2; 2_1^+ \to 0_{gs}^+)$ values which has been a topic of several works. Although established interactions were able to describe the excitations energies in these Ti isotopes and the structure in the neighboring nuclei they were generally unable to exactly reproduce the experimental $B(E2; 2_1^+ \to 0_{gs}^+)$ values in neutron-rich Ti isotopes even using isoscalar proton and neutron effective charges [10, 42, 44]. The new $B(E2; 2_1^+ \to 0_{gs}^+)$ systematics for $^{50-54}$Ti (see Fig. 11) exhibit a clearly weaker staggering with flat amplitude in $N = 30$. The $B(E2; 2_1^+ \to 0_{gs}^+)$ values for most of interactions are very similar for $^{50-54}$Ti. A splitting in the $B(E2; 2_1^+ \to 0_{gs}^+)$ trends becomes apparent for ^{56}Ti, where the GXPF1A and GXPF1B differ clearly from each other, with the latter one showing an increased value closer to experiment. Since the GXPF1B interaction was optimized to describe the local subshell closure $N = 34$ in ^{54}Ca [40], it is not surprising that it also reproduces the isotone ^{56}Ti better than GXPF1A. The KB3G interaction yields a similar good description for $^{52-56}$Ti. Returning to ^{50}Ti ($N = 28$) there is clear over-prediction of the $B(E2; 2_1^+ \to 0_{gs}^+)$ values by all shell-model interactions. One possible explanation are proton particle hole excitations across the $Z = 20$ ^{40}Ca core present in the 0_{gs}^+ state, which are not accounted for in this model space, and to lesser extent in the 2_1^+ state leading to an over-prediction of the $E2$ strength. Another explanation is given by the inspection of the wave function of 0_{gs}^+ and 2_1^+ states in ^{50}Ti in the GXPF1A/(B) calculations which predict about 30 % (38 %) configurations with neutron particle hole excitations across the $N = 28$ shell, which increase the specific $E2$ strength. Therefore to reduce the $E2$ strength from neutron $N = 28$ cross-shell excitations an 'ad-hoc' modification of the GXPF1B interaction was defined, called GXPF1B-nf7, where the single particle energy of the $\nu 1f_{7/2}$ orbital was lowered by 1 MeV. The results for GXPF1B-nf7 are presented and compared to the experiment and the other interactions (see Fig. 11, 12 and Table III). This interaction has only a qualitative value, but maybe relevant for $^{50-52}$Ti and generally achieves the best results for the $^{50-56}$Ti $B(E2; 2_1^+ \to 0_{gs}^+)$ systematics. The transition strengths in the calculations are computed according to $B(E2; I_1^+ \to (I-2)_1^+) = [A_p * e_\pi + A_n * e_\nu]^2/(2\,I_1 + 1)$ [45], with the proton and neutron amplitudes A_p and A_n in units of fm^2. A summary of the these proton and neutron amplitudes of the $2_1^+ \to 0_{gs}$ transitions in $^{50-56}$Ti for four different interactions is given in Table IV. Small A_n amplitudes are characteristic of shell gaps at $N = 28$ and $N = 32$, as already discussed in Ref. [10].

Thus the general flat $B(E2; 2_1^+ \to 0_{gs}^+)$ trends of the shell model could be understood by the fine balance of proton and neutron amplitudes, for which the variation of the A_n is compensated by the anti-variation of A_p, leading to constant $B(E2; 2_1^+ \to 0_{gs}^+)$ values for these effective charges. Thus, regarding the systematics of the lowest transition strengths, a consistent picture between experimental and theoretical results emerges.

Table III. Experimental excitation energies for the 2_1^+, 4_1^+ and 6_1^+ states in ^{50,52,54,56}Ti are compared to the energies of six different shell-model calculations. For a better comparison the χ^2 deviation for each interaction is determined.

	Excitation energy E [keV]												
	^{50}Ti			^{52}Ti			^{54}Ti			^{56}Ti			
	2_1^+	4_1^+	6_1^+	2_1^+	4_1^+	6_1^+	2_1^+	4_1^+	6_1^+	2_1^+	4_1^+	6_1^+	χ^2
Experiment	1553	2675	3199	1050	2318	3029	1495	2496	2936	1128	2288	2978	-
GXPF1A	1624	2562	3237	1106	2251	2932	1395	2465	2975	1176	2278	2868	30.2
GXPF1B	1626	2568	3234	1084	2239	2922	1434	2476	2974	1134	2296	2873	22.6
GXPF1B-nf7	1699	2572	3153	1089	2229	2899	1416	2468	2965	1215	2312	2900	42.6
KB3G	1715	2841	3383	1069	2356	3048	1285	2452	3048	886	1995	2873	166.6

In the following, the higher spins in the even $^{50-54}$Ti are discussed. Due to the similar behavior between GXPF1A and GXPF1B for these isotopes, only GXPF1B is discussed below.

Figure 12 shows a comparison between the experimental results and the shell-model calculations for the $B(E2; I_1^+ \rightarrow (I-2)_1^+)$ values in ^{50,52,54}Ti (for the sake of clarity GXPF1A is not listed due to similar results).

In ^{50}Ti the experimental $B(E2; 2_1^+ \rightarrow 0_{gs}^+)$ value from Ref. [46] is slightly overestimated by the established interactions. This could be attributed to proton particle hole excitations across the $Z = 20$ ^{40}Ca core present in the 0_{gs}^+ state, which are not accounted for in this model space, or as discussed above the $B(E2)$ could be overestimated due to the degree of neutron particle hole excitation across $N = 28$ as qualitatively demonstrated by GXPF1B-nf7 calculation. The adopted $B(E2; 4_1^+ \rightarrow 2_1^+)$ and $B(E2; 6_1^+ \rightarrow 4_1^+)$ values agree well with the theoretical predictions of all interactions with only marginal difference. The shell-model calculations predict that the $I = 2_1^+, 4_1^+, 6_1^+$ states in ^{50}Ti have proton character dominated by $\geq 70\,\%$ configurations of the type $\pi_{I^+} \otimes \nu_{0^+}$.

Table IV. Proton and neutron amplitudes for the $2_1^+ \rightarrow 0_{gs}^+$ of four different interactions for even $^{50-56}$Ti.

$2^+ \rightarrow 0_{gs}^+$	^{50}Ti		^{52}Ti		^{54}Ti		^{56}Ti	
	A_p	A_n	A_p	A_n	A_p	A_n	A_p	A_n
GXPF1A	11.59	10.06	9.96	15.17	11.54	10.62	11.02	12.21
GXPF1B	11.58	10.01	9.66	15.19	11.72	9.81	11.31	14.43
GXPF1B-nf7	11.83	7.12	9.84	14.36	11.76	9.82	11.72	12.16
KB3G	11.87	9.21	9.37	15.70	10.76	12.24	10.30	18.09

For the neighboring nucleus ^{52}Ti the results of the calculations generally agree well with the new $B(E2)$ values (cf. Fig. 12). Only the $B(E2; 2_1^+ \rightarrow 0_{gs}^+)$ and $B(E2; 6_1^+ \rightarrow 4_1^+)$ values are slightly overestimated or underestimated. In contrast to ^{50}Ti the wave function of $I = 2_1^+$ state has dominant neutron character with $\sim 50\,\%$ $\pi_{0^+} \otimes \nu_{2^+}$ and $\sim 30\,\%$ $\pi_{2^+} \otimes \nu_{0^+}$ configuration. The two neutrons above $N = 28$ occupy predominantly the $2p_{3/2}$ orbital in which they can couple to a maximum of $2\hbar$. Therefore the higher spin yrast states $I = 4^+, 6^+$, cannot be of pure neutron character. For $I = 4^+$ mixed proton-neutron configurations $\sim 30\,\%$ $\pi_{2^+} \otimes \nu_{2^+}$ and $\sim 40\,\%$ $\pi_{4^+} \otimes \nu_{0^+}$ for KB3G and GXPF1B are prevailing. For $I = 6^+$ the wave functions of the three interactions are similar. The configuration $\pi_{6^+} \otimes \nu_{0^+}$ has the largest contribution to the wave function ($\leq 50\,\%$), followed by the mixed configurations of type $\pi_{4^+} \otimes \nu_{2^+}$ and $\pi_{6^+} \otimes \nu_{2^+}$ ($\leq 12\,\%$). We note the very good agreement between the new experimental $B(E2)$ values from this work and the theory both having the opposite trend to the adopted data from Ref. [22]. The new results could clarify the long-standing contradiction between the shell model and adopted $B(E2; 2_1^+ \rightarrow 0_{gs}^+)$ in ^{52}Ti, thus refuting the previous experimental results.

In ^{54}Ti, i.e. four neutrons above $N = 28$, all interactions reproduce fairly accurately the $B(E2; 2_1^+ \rightarrow 0_{gs}^+)$ value from Ref. [10] and yield very similar $B(E2; 4_1^+ \rightarrow 2_1^+)$ values. However, they all clearly underestimate the experimental value of $B(E2; 4_1^+ \rightarrow 2_1^+) = 139^{+25}_{-18}\, e^2\mathrm{fm}^4$ determined in this work. For the $6_1^+ \rightarrow 4_1^+$ transition the calculations yield $B(E2)$ values half the size of the $4_1^+ \rightarrow 2_1^+$ and $2_1^+ \rightarrow 0_{gs}^+$ transitions. From the experimental data an upper limit of $B(E2; 6_1^+ \rightarrow 4_1^+) \leq 132\, e^2\mathrm{fm}^4$ was determined, so that the results of the calculations are in agreement. In addition, the experimental result of a lower limit of $B(E2; 8_1^+ \rightarrow 6_1^+) \geq 5.7\, e^2\mathrm{fm}^4$ agrees with GXPF1B. The wave functions of KB3G and GXPF1B show a distinct proton occupation similar to ones in ^{50}Ti. For the 2_1^+ state the proton occupation yields $\sim 50\,\%$ $\pi_{2^+} \otimes \nu_{0^+}$ corresponding to a subshell closure of $\nu 2p_{3/2}$. This confirms that the $p_{3/2}$ and $f_{5/2}$ orbitals are not close to each other. Also the other higher-lying states $I = 4_1^+, 6_1^+$ show clear proton character ($\sim 60\,\%$ $\pi_{4^+} \otimes \nu_{0^+}$ and $\geq 70\,\%$ $\pi_{6^+} \otimes \nu_{0^+}$ for KB3G and GXPF1B). In ^{54}Ti the trend of the shell-model $B(E2; I_1^+ \rightarrow (I-2)_1^+)$ resembles the trend in ^{50}Ti which is another signature of the

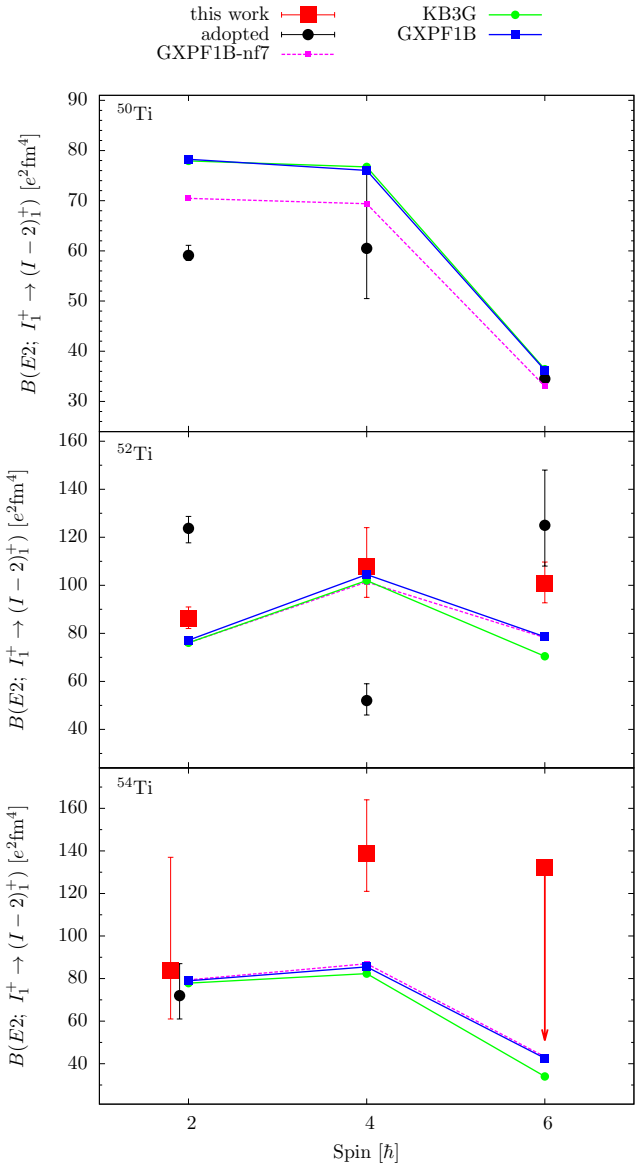

Figure 12. (Color online) Comparison of experimental $B(E2; I_1^+ \rightarrow (I-2)_1^+)$ values in ^{50,52,54}Ti with results of different theoretical approaches. See text for details.

$N = 32$ subshell closure demonstrated in the shell-model results.

V. SUMMARY

Summarizing, the structure of neutron-rich nuclei ^{52,54}Ti was investigated via multinucleon-transfer reactions in inverse kinematics. In ^{54}Ti the lifetime of the 2_1^+ state was remeasured. The obtained value confirms the result from an earlier experiment with Coulomb excitation [10]. The lifetime of the 4_1^+ state, a lower limit for that of the 6_1^+ state and an upper limit of that of the 8_1^+ state were determined for the first time.

The comparison with shell-model calculations shows the following outcome: In ^{54}Ti the trend of the $B(E2; I_1^+ \rightarrow (I-2)^+)$ values agree well with the results of different shell-model calculations, only the experimental result of the $B(E2; 4_1^+ \rightarrow 2_1^+)$ value is underestimated.

In ^{52}Ti lifetime values of the $2_1^+, 4_1^+$ and 6_1^+ states were remeasured with an astonishing result. The transition probabilities obtained from the lifetimes determined in this work show an opposite trend to the existing $B(E2; I_1^+ \rightarrow (I-2)_1^+)$ values known from the literature. The $B(E2; 2_1^+ \rightarrow 0_{gs}^+)$ value is clearly below the adopted value. Same behavior was achieved for the $6_1^+ \rightarrow 4_1^+$ transition. In contrast, the new $B(E2; 4_1^+ \rightarrow 2_1^+)$ is clearly higher than the adopted value. In contrast to the previously known results for ^{52}Ti the new results on $B(E2; I_1^+ \rightarrow (I-2)_1^+)$ values are well reproduced within the shell model. Compared to neighboring findings, the new $B(E2; 2_1^+ \rightarrow 0_{gs}^+)$ results do not show a staggering along the titanium isotopic chain $^{50-54}$Ti. The experimental and theoretical results confirm a subshell closure at $N = 32$ in ^{54}Ti.

ACKNOWLEDGMENTS

We thank the GANIL team for the professional support during the experiment. The research leading to these results has received funding from the German BMBF under contract No. 05P18PKFN9.

[1] B. A. Brown, "The nuclear shell model towards the drip lines," Progress in Particle and Nuclear Physics **47**, 517–599 (2001).

[2] T. Braunroth, A. Dewald, H. Iwasaki, S. M. Lenzi, M. Albers, V. M. Bader, T. Baugher, T. Baumann, D. Bazin, J. S. Berryman, C. Fransen, A. Gade, T. Ginter, A. Gottardo, M. Hackstein, J. Jolie, A. Lemasson, J. Litzinger, S. Lunardi, T. Marchi, V. Modamio, C. Morse, D. R. Napoli, A. Nichols, F. Recchia, S. R. Stroberg, R. Wadsworth, D. Weisshaar, K. Whitmore, and K. Wimmer, "Reduced transition strengths of low-lying yrast states in chromium isotopes in the vicinity of $N = 40$," Phys. Rev. C **92**, 034306 (2015).

[3] A. Gade, R. V. F. Janssens, T. Baugher, D. Bazin, B. A. Brown, M. P. Carpenter, C. J. Chiara, A. N. Deacon, S. J. Freeman, G. F. Grinyer, C. R. Hoffman, B. P. Kay, F. G. Kondev, T. Lauritsen, S. McDaniel, K. Meierbachtol, A. Ratkiewicz, S. R. Stroberg, K. A. Walsh, D. Weisshaar, R. Winkler, and S. Zhu, "Collectivity at $N = 40$ in neutron-rich ^{64}Cr," Phys. Rev. C **81**, 051304 (2010).

[4] S. M. Lenzi, F. Nowacki, A. Poves, and K. Sieja, "Island of inversion around ^{64}Cr," Phys. Rev. C **82**, 054301

(2010).
[5] C. Santamaria, C. Louchart, A. Obertelli, V. Werner, P. Doornenbal, F. Nowacki, G. Authelet, H. Baba, D. Calvet, F. Château, A. Corsi, A. Delbart, J.-M. Gheller, A. Gillibert, T. Isobe, V. Lapoux, M. Matsushita, S. Momiyama, T. Motobayashi, M. Niikura, H. Otsu, C. Péron, A. Peyaud, E. C. Pollacco, J.-Y. Roussé, H. Sakurai, M. Sasano, Y. Shiga, S. Takeuchi, R. Taniuchi, T. Uesaka, H. Wang, K. Yoneda, F. Browne, L. X. Chung, Zs. Dombradi, S. Franchoo, F. Giacoppo, A. Gottardo, K. Hadynska-Klek, Z. Korkulu, S. Koyama, Y. Kubota, J. Lee, M. Lettmann, R. Lozeva, K. Matsui, T. Miyazaki, S. Nishimura, L. Olivier, S. Ota, Z. Patel, N. Pietralla, E. Sahin, C. Shand, P.-A. Söderström, I. Stefan, D. Steppenbeck, T. Sumikama, D. Suzuki, Zs. Vajta, J. Wu, and Z. Xu, "Extension of the $N = 40$ Island of Inversion towards $N = 50$: Spectroscopy of ^{66}Cr, ^{70,72}Fe," Phys. Rev. Lett. **115**, 192501 (2015).
[6] W. Rother, A. Dewald, H. Iwasaki, S. M. Lenzi, K. Starosta, D. Bazin, T. Baugher, B. A. Brown, H. L. Crawford, C. Fransen, A. Gade, T. N. Ginter, T. Glasmacher, G. F. Grinyer, M. Hackstein, G. Ilie, J. Jolie, S. McDaniel, D. Miller, P. Petkov, Th. Pissulla, A. Ratkiewicz, C. A. Ur, P. Voss, K. A. Walsh, D. Weisshaar, and K. O. Zell, "Enhanced Quadrupole Collectivity at $N = 40$: The Case of Neutron-Rich Fe Isotopes," Phys. Rev. Lett. **106**, 022502 (2011).
[7] J. Ljungvall, A. Görgen, A. Obertelli, W. Korten, E. Clément, G. de France, A. Bürger, J.-P. Delaroche, A. Dewald, A. Gadea, L. Gaudefroy, M. Girod, M. Hackstein, J. Libert, D. Mengoni, F. Nowacki, T. Pissulla, A. Poves, F. Recchia, M. Rejmund, W. Rother, E. Sahin, C. Schmitt, A. Shrivastava, K. Sieja, J. J. Valiente-Dobón, K. O. Zell, and M. Zielińska, "Onset of collectivity in neutron-rich Fe isotopes: Toward a new island of inversion?" Phys. Rev. C **81**, 061301 (2010).
[8] H. L. Crawford, R. M. Clark, P. Fallon, A. O. Macchiavelli, T. Baugher, D. Bazin, C. W. Beausang, J. S. Berryman, D. L. Bleuel, C. M. Campbell, M. Cromaz, G. de Angelis, A. Gade, R. O. Hughes, I. Y. Lee, S. M. Lenzi, F. Nowacki, S. Paschalis, M. Petri, A. Poves, A. Ratkiewicz, T. J. Ross, E. Sahin, D. Weisshaar, K. Wimmer, and R. Winkler, "Quadrupole collectivity in neutron-rich fe and cr isotopes," Phys. Rev. Lett. **110**, 242701 (2013).
[9] D. Steppenbeck, S. Takeuchi, N. Aoi, P. Doornenbal, M. Matsushita, H. Wang, H. Baba, N. Fukuda, S. Go, M. Honma, J. Lee, K. Matsui, S. Michimasa, T. Motobayashi, D. Nishimura, T. Otsuka, H. Sakurai, Y. Shiga, P.-A. Söderström, T. Sumikama, H. Suzuki, R. Taniuchi, Y. Utsuno, J. J. Valiente-Dobón, and K. Yoneda, "Evidence for a new nuclear 'magic number' from the level structure of ^{54}Ca," Nature **502**, 207 (2013).
[10] D.-C. Dinca, R. V. F. Janssens, A. Gade, D. Bazin, R. Broda, B. A. Brown, C. M. Campbell, M. P. Carpenter, P. Chowdhury, J. M. Cook, A. N. Deacon, B. Fornal, S. J. Freeman, T. Glasmacher, M. Honma, F. G. Kondev, J.-L. Lecouey, S. N. Liddick, P. F. Mantica, W. F. Mueller, H. Olliver, T. Otsuka, J. R. Terry, B. A. Tomlin, and K. Yoneda, "Reduced transition probabilities to the first 2^+ state in ^{52,54,56}Ti and development of shell closures at $N = 32, 34$," Phys. Rev. C **71**, 041302 (2005).
[11] H. Hübel, A. Bürger, T. R. Saito, H. Grawe, P. Reiter, J. Gerl, M. Górska, H. J. Wollersheim, A. Al-Khatib, A. Banu, T. Beck, F. Becker, P. Bednarczyk, G. Benzoni, A. Bracco, S. Brambilla, P. Bringel, F. Camera, E. Clément, P. Doornenbal, H. Geissel, A. Görgen, J. Grębosz, G. Hammond, M. Hellström, M. Kavatsyuk, O. Kavatsyuk, M. Kmiecik, I. Kojouharov, W. Korten, N. Kurz, R. Lozeva, A. Maj, S. Mandal, B. Million, S. Muralithar, A. Neußer-Neffgen, Zs. Podolyák, N. Saito, A. K. Singh, H. Weick, O. Wieland, M. Winkler, and C. Wheldon, "Relativistic coulomb excitation of neutron-rich ^{54,56,58}Cr," Acta Physica Hungarica A) Heavy Ion Physics **25**, 197 (2006).
[12] M. Seidlitz, P. Reiter, A. Dewald, O. Möller, B. Bruyneel, S. Christen, F. Finke, C. Fransen, M. Górska, H. Grawe, A. Holler, G. Ilie, T. Kotthaus, P. Kudejová, S. M. Lenzi, S. Mandal, B. Melon, D. Mücher, J.-M. Regis, B. Saha, P. von Brentano, A. Wiens, and K. O. Zell, "Precision lifetime measurements of the first 2^+ and 4^+ states in ^{56}Cr at the $N = 32$ subshell closure," Phys. Rev. C **84**, 034318 (2011).
[13] M. J. LeVine, E. K. Warburton, and D. Schwalm, "Static quadrupole moments for the 2^+ states of ^{54,56,58}Fe," Phys. Rev. C **23**, 244–252 (1981).
[14] O. Kenn, K.-H. Speidel, R. Ernst, J. Gerber, P. Maier-Komor, and F. Nowacki, "Measurements of g factors and lifetimes of low lying states in $^{58-64}$Ni and their shell model implications," Phys. Rev. C **63**, 064306 (2001).
[15] R. V. F. Janssens, B. Fornal, P. F Mantica, B. A Brown, R. Broda, P. Bhattacharyya, M. Carpenter, M. Cinausero, P. J. Daly, A. D. Davies, T. Glasmacher, Z. W. Grabowski, D. E. Groh, M. Honma, F. Kondev, W. Królas, T. Lauritsen, S. N. Liddick, S. Lunardi, and J. Wrzesiński, "Structure of ^{52,54}Ti and shell closures in neutron-rich nuclei above ^{48}Ca," Physics Letters B **546**, 55–62 (2002).
[16] B. Fornal, S. Zhu, R. V. F. Janssens, M. Honma, R. Broda, P. F. Mantica, B. A. Brown, M. P. Carpenter, P. J. Daly, S. J. Freeman, Z. W. Grabowski, N. J. Hammond, F. G. Kondev, W. Królas, T. Lauritsen, S. N. Liddick, C. J. Lister, E. F. Moore, T. Otsuka, T. Pawłat, D. Seweryniak, B. E. Tomlin, and J. Wrzesiński, "Development of shell closures at $N = 32, 34$. II. Lowest yrast excitations in even-even Ti isotopes from deep-inelastic heavy-ion collisions," Phys. Rev. C **70**, 064304 (2004).
[17] A. Huck, G. Klotz, A. Knipper, C. Miehé, C. Richard-Serre, G. Walter, A. Poves, H. L. Ravn, and G. Marguier, "Beta decay of the new isotopes ^{52}K, ^{52}Ca, and ^{52}Sc; a test of the shell model far from stability," Phys. Rev. C **31**, 2226–2237 (1985).
[18] S. N. Liddick, P. F. Mantica, R. Broda, B. A. Brown, M. P. Carpenter, A. D. Davies, B. Fornal, T. Glasmacher, D. E. Groh, M. Honma, M. Horoi, R. V. F. Janssens, T. Mizusaki, D. J. Morrissey, A. C. Morton, W. F. Mueller, T. Otsuka, J. Pavan, H. Schatz, A. Stolz, S. L. Tabor, B. E. Tomlin, and M. Wiedeking, "Development of shell closures at $N = 32, 34$. I. β decay of neutron-rich Sc isotopes," Phys. Rev. C **70**, 064303 (2004).
[19] T. Otsuka, T. Suzuki, R. Fujimoto, H. Grawe, and Y. Akaishi, "Evolution of Nuclear Shells due to the Tensor Force," Phys. Rev. Lett. **95**, 232502 (2005).
[20] T. Otsuka, R. Fujimoto, Y. Utsuno, B. A. Brown, M. Honma, and T. Mizusaki, "Magic Numbers in Exotic Nuclei and Spin-Isospin Properties of the NN Interaction," Phys. Rev. Lett. **87**, 082502 (2001).

[21] T. Otsuka, T. Suzuki, M. Honma, Y. Utsuno, N. Tsunoda, K. Tsukiyama, and M. Hjorth-Jensen, "Novel Features of Nuclear Forces and Shell Evolution in Exotic Nuclei," Phys. Rev. Lett. **104**, 012501 (2010).

[22] K.-H. Speidel, J. Leske, S. Schielke, S. C. Bedi, O. Zell, P. Maier-Komor, S. J. Q. Robinson, Y. Y. Sharon, and L. Zamick, "Low-level structure of 52Ti based on g factor and lifetime measurements," Physics Letters B **633**, 219 – 224 (2006).

[23] A. Dewald, O. Möller, and P. Petkov, "Developing the Recoil Distance Doppler-Shift technique towards a versatile tool for lifetime measurements of excited nuclear states," Progress in Particle and Nuclear Physics **67**, 786–839 (2012).

[24] S. Pullanhiotan, M. Rejmund, A. Navin, W. Mittig, and S. Bhattacharyya, "Performance of VAMOS for reactions near the Coulomb barrier," Nuclear Instruments and Methods in Physics Research Section A: Accelerators, Spectrometers, Detectors and Associated Equipment **593**, 343 – 352 (2008).

[25] M. Rejmund, B. Lecornu, A. Navin, C. Schmitt, S. Damoy, O. Delaune, J.M. Enguerrand, G. Fremont, P. Gangnant, L. Gaudefroy, B. Jacquot, J. Pancin, S. Pullanhiotan, and C. Spitaels, "Performance of the improved larger acceptance spectrometer: VAMOS++," Nuclear Instruments and Methods in Physics Research Section A: Accelerators, Spectrometers, Detectors and Associated Equipment **646**, 184 – 191 (2011).

[26] M. Vandebrouck, A. Lemasson, M. Rejmund, G. Frémont, J. Pancin, A. Navin, C. Michelagnoli, J. Goupil, C. Spitaels, and B. Jacquot, "Dual Position Sensitive MWPC for tracking reaction products at VAMOS++," Nuclear Instruments and Methods in Physics Research Section A: Accelerators, Spectrometers, Detectors and Associated Equipment **812**, 112–117 (2016).

[27] Y. H. Kim, A. Lemasson, M. Rejmund, A. Navin, S. Biswas, C. Michelagnoli, I. Stefan, R. Banik, P. Bednarczyk, S. Bhattacharya, S. Bhattacharyya, E. Clément, H. L. Crawford, G. De France, P. Fallon, J. Goupil, B. Jacquot, H. J. Li, J. Ljungvall, A. O. Macchiavelli, A. Maj, L. Ménager, V. Morel, R. Palit, R. M. Pérez-Vidal, J. Ropert, and C. Schmitt, "Prompt-delayed $\gamma\gamma$-ray spectroscopy with AGATA, EXOGAM and VAMOS++," The European Physical Journal A **53**, 162 (2017).

[28] S. Akkoyun, A. Algora, B. Alikhani, F. Ameil, G. de Angelis, L. Arnold, A. Astier, A. Ataç, Y. Aubert, C. Aufranc, A. Austin, S. Aydin, F. Azaiez, S. Badoer, D.L. Balabanski, D. Barrientos, G. Baulieu, R. Baumann, D. Bazzacco, F. A. Beck, T. Beck, P. Bednarczyk, M. Bellato, M. A. Bentley, G. Benzoni, R. Berthier, L. Berti, R. Beunard, G. Lo Bianco, B. Birkenbach, P. G. Bizzeti, A. M. Bizzeti-Sona, F. Le Blanc, J.M. Blasco, N. Blasi, D. Bloor, C. Boiano, M. Borsato, D. Bortolato, A. J. Boston, H. C. Boston, P. Bourgault, P. Boutachkov, A. Bouty, A. Bracco, S. Brambilla, I. P. Brawn, A. Brondi, S. Broussard, B. Bruyneel, D. Bucurescu, I. Burrows, A. Bürger, S. Cabaret, B. Cahan, E. Calore, F. Camera, A. Capsoni, F. Carrió, G. Casati, M. Castoldi, B. Cederwall, J.-L. Cercus, V. Chambert, M. El Chambit, R. Chapman, L. Charles, J. Chavas, E. Clément, P. Cocconi, S. Coelli, P. J. Coleman-Smith, A. Colombo, S. Colosimo, C. Commeaux, D. Conventi, R. J. Cooper, A. Corsi, A. Cortesi, L. Costa, F. C. L. Crespi, J. R. Cresswell, D.M. Cullen, D. Curien, A. Czermak, D. Delbourg, R. Depalo, T. Descombes, P. Désesquelles, P. Detistov, C. Diarra, F. Didierjean, M. R. Dimmock, Q. T. Doan, C. Domingo-Pardo, M. Doncel, F. Dorangeville, N. Dosme, Y. Drouen, G. Duchâne, B. Dulny, J. Eberth, P. Edelbruck, J. Egea, T. Engert, M. N. Erduran, S. Ertürk, C. Fanin, S. Fantinel, E. Farnea, T. Faul, M. Filliger, F. Filmer, Ch. Finck, G. de France, A. Gadea, W. Gast, A. Geraci, J. Gerl, R. Gernhäuser, A. Giannatiempo, A. Giaz, L. Gibelin, A. Givechev, N. Goel, V. González, A. Gottardo, X. Grave, J. Grebosz, R. Griffiths, A. N. Grint, P. Gros, L. Guevara, M. Gulmini, A. Görgen, H. T. M. Ha, T. Habermann, L. J. Harkness, H. Harroch, K. Hauschild, C. He, A. Hernández-Prieto, B. Hervieu, H. Hess, T. Hüyük, E. Ince, R. Isocrate, G. Jaworski, A. Johnson, J. Jolie, P. Jones, B. Jonson, P. Joshi, D. S. Judson, A. Jungclaus, M. Kaci, N. Karkour, M. Karolak, A. Kaşkaş, M. Kebbiri, R. S. Kempley, A. Khaplanov, S. Klupp, M. Kogimtzis, I. Kojouharov, A. Korichi, W. Korten, Th. Kröll, R. Krücken, N. Kurz, B.Y. Ky, M. Labiche, X. Lafay, L. Lavergne, I.H. Lazarus, S. Leboutelier, F. Lefebvre, E. Legay, L. Legeard, F. Lelli, S. M. Lenzi, S. Leoni, A. Lermitage, D. Lersch, J. Leske, S. C. Letts, S. Lhenoret, R. M. Lieder, D. Linget, J. Ljungvall, A. Lopez-Martens, A. Lotodé, S. Lunardi, A. Maj, J. van der Marel, Y. Mariette, N. Marginean, R. Marginean, G. Maron, A. R. Mather, W. Meczyński, V. Mendéz, P. Medina, B. Melon, R. Menegazzo, D. Mengoni, E. Merchan, L. Mihailescu, C. Michelagnoli, J. Mierzejewski, L. Milechina, B. Million, K. Mitev, P. Molini, D. Montanari, S. Moon, F. Morbiducci, R. Moro, P. S. Morrall, O. Möller, A. Nannini, D. R. Napoli, L. Nelson, M. Nespolo, V. L. Ngo, M. Nicoletto, R. Nicolini, Y. Le Noa, P. J. Nolan, M. Norman, J. Nyberg, A. Obertelli, A. Olariu, R. Orlandi, D. C. Oxley, C. Özben, M. Ozille, C. Oziol, E. Pachoud, M. Palacz, J. Palin, J. Pancin, C. Parisel, P. Pariset, G. Pascovici, R. Peghin, L. Pellegri, A. Perego, S. Perrier, M. Petcu, P. Petkov, C. Petrache, E. Pierre, N. Pietralla, S. Pietri, M. Pignanelli, I. Piqueras, Z. Podolyak, P. Le Pouhalec, J. Pouthas, D. Pugnére, V. F. E. Pucknell, A. Pullia, B. Quintana, R. Raine, G. Rainovski, L. Ramina, G. Rampazzo, G. La Rana, M. Rebeschini, F. Recchia, N. Redon, M. Reese, P. Reiter, P.H. Regan, S. Riboldi, M. Richer, M. Rigato, S. Rigby, G. Ripamonti, A.P. Robinson, J. Robin, J. Roccaz, J.-A. Ropert, B. Rossé, C. Rossi Alvarez, D. Rosso, B. Rubio, D. Rudolph, F. Saillant, E. Şahin, F. Salomon, M.-D. Salsac, J. Salt, G. Salvato, J. Sampson, E. Sanchis, C. Santos, H. Schaffner, M. Schlarb, D. P. Scraggs, D. Seddon, M. Şenyiğit, M.-H. Sigward, G. Simpson, J. Simpson, M. Slee, J.F. Smith, P. Sona, B. Sowicki, P. Spolaore, C. Stahl, T. Stanios, E. Stefanova, O. Stézowski, J. Strachan, G. Suliman, P.-A. Söderström, J. L. Tain, S. Tanguy, S. Tashenov, Ch. Theisen, J. Thornhill, F. Tomasi, N. Toniolo, R. Touzery, B. Travers, A. Triossi, M. Tripon, K. M. M. Tun-Lanoë, M. Turcato, C. Unsworth, C. A. Ur, J. J. Valiente-Dobón, V. Vandone, E. Vardaci, R. Venturelli, F. Veronese, Ch. Veyssiere, E. Viscione, R. Wadsworth, P. M. Walker, N. Warr, C. Weber, D. Weisshaar, D. Wells, O. Wieland, A. Wiens, G. Wittwer, H. J. Wollersheim, F. Zocca, N. V. Zamfir, M. Ziebliński, and A. Zucchiatti, "AGATA-

Advanced GAmma Tracking Array," Nuclear Instruments and Methods in Physics Research Section A: Accelerators, Spectrometers, Detectors and Associated Equipment **668**, 26 – 58 (2012).

[29] E. Clément, C. Michelagnoli, G. de France, H. J. Li, A. Lemasson, C. Barthe Dejean, M. Beuzard, P. Bougault, J. Cacitti, J.-L. Foucher, G. Fremont, P. Gangnant, J. Goupil, C. Houarner, M. Jean, A. Lefevre, L. Legeard, F. Legruel, C. Maugeais, L. Ménager, N. Ménard, H. Munoz, M. Ozille, B. Raine, J.A. Ropert, F. Saillant, C. Spitaels, M. Tripon, Ph. Vallerand, G. Voltolini, W. Korten, M.-D. Salsac, Ch. Theisen, M. Zielińska, T. Joannem, M. Karolak, M. Kebbiri, A. Lotode, R. Touzery, Ch. Walter, A. Korichi, J. Ljungvall, A. Lopez-Martens, D. Ralet, N. Dosme, X. Grave, N. Karkour, X. Lafay, E. Legay, I. Kojouharov, C. Domingo-Pardo, A. Gadea, R.M. Pérez-Vidal, J.V. Civera, B. Birkenbach, J. Eberth, H. Hess, L. Lewandowski, P. Reiter, A. Nannini, G. De Angelis, G. Jaworski, P. John, D.R. Napoli, J. J. Valiente-Dobón, D. Barrientos, D. Bortolato, G. Benzoni, A. Bracco, S. Brambilla, F. Camera, F.C.L. Crespi, S. Leoni, B. Million, A. Pullia, O. Wieland, D. Bazzacco, S. M. Lenzi, S. Lunardi, R. Menegazzo, D. Mengoni, F. Recchia, M. Bellato, R. Isocrate, F. J. Egea Canet, F. Didierjean, G. Duchˆene, R. Baumann, M. Brucker, E. Dangelser, M. Filliger, H. Friedmann, G. Gaudiot, J.-N. Grapton, H. Kocher, C. Mathieu, M.-H. Sigward, D. Thomas, S. Veeramootoo, J. Dudouet, O. Stézowski, C. Aufranc, Y. Aubert, M. Labiche, J. Simpson, I. Burrows, P. J. Coleman-Smith, A. Grant, I. H. Lazarus, P. S. Morrall, V. F. E. Pucknell, A. Boston, D. S. Judson, N. Lalović, J. Nyberg, J. Collado, V. González, I. Kuti, B. M. Nyakó, A. Maj, and M. Rudigier, "Conceptual design of the AGATA 1π array at GANIL," Nuclear Instruments and Methods in Physics Research Section A: Accelerators, Spectrometers, Detectors and Associated Equipment **855**, 1 – 12 (2017).

[30] Z. G. Wang, C. Dufour, E. Paumier, and M. Toulemonde, "The Se sensitivity of metals under swift-heavy-ion irradiation: a transient thermal process," Journal of Physics: Condensed Matter **6**, 6733 (1994).

[31] M. Toulemonde, E. Paumier, and C. Dufour, "Thermal spike model in the electronic stopping power regime," Radiation Effects and Defects in Solids **126**, 201–206 (1993).

[32] A. Goldkuhle, C. Fransen, A. Dewald, K. Arnswald, M. Bast, M. Beckers, A. Blazhev, T. Braunroth, G. Hackenberg, G. Häfner, J. Litzinger, J. Jolie, C. Müller-Gatermann, F. von Spee, N. Warr, D. Werner, and K. O. Zell, "Lifetime measurement of excited states in ^{46}Ti," The European Physical Journal A **55**, 53 (2019).

[33] T. Braunroth, private communication (2018).

[34] A. Dewald, S. Harissopulos, and P. von Brentano, "The differential plunger and the differential decay curve method for the analysis of recoil distance Doppler-shift data," Zeitschrift für Physik A Atomic Nuclei **334**, 163–175 (1989).

[35] B. Saha, "Computer code NAPATAU, unpublished," .

[36] E. Leistenschneider, M. P. Reiter, S. Ayet San Andrés, B. Kootte, J. D. Holt, P. Navrátil, C. Babcock, C. Barbieri, B. R. Barquest, J. Bergmann, J. Bollig, T. Brunner, E. Dunling, A. Finlay, H. Geissel, L. Graham, F. Greiner, H. Hergert, C. Hornung, C. Jesch, R. Klawitter, Y. Lan, D. Lascar, K. G. Leach, W. Lippert, J. E. McKay, S. F. Paul, A. Schwenk, D. Short, J. Simonis, V. Somà, R. Steinbrügge, S. R. Stroberg, R. Thompson, M. E. Wieser, C. Will, M. Yavor, C. Andreoiu, T. Dickel, I. Dillmann, G. Gwinner, W. R. Plaß, C. Scheidenberger, A. A. Kwiatkowski, and J. Dilling, "Dawning of the $N = 32$ Shell Closure Seen through Precision Mass Measurements of Neutron-Rich Titanium Isotopes," Phys. Rev. Lett. **120**, 062503 (2018).

[37] B. A. Brown and W. D. M. Rae, "The Shell-Model Code NuShellX@MSU," Nuclear Data Sheets **120**, 115–118 (2014).

[38] A. Poves, J. Sánchez-Solano, E. Caurier, and F. Nowacki, "Shell model study of the isobaric chains $A = 50$, $A = 51$ and $A = 52$," Nuclear Physics A **694**, 157 – 198 (2001).

[39] M. Honma, T. Otsuka, B. A. Brown, and T. Mizusaki, "Shell-model description of neutron-rich pf-shell nuclei with a new effective interaction GXPF 1," The European Physical Journal A - Hadrons and Nuclei **25**, 499–502 (2005).

[40] M. Honma, T. Otsuka, and T. Mizusaki, "Shell-model description of neutron-rich Ca isotopes," RIKEN Accel. Prog. Rep. **41** (2008).

[41] M. Dufour and A. P. Zuker, "Realistic collective nuclear Hamiltonian," Phys. Rev. C **54**, 1641–1660 (1996).

[42] J. J. Valiente-Dobón, D. Mengoni, A. Gadea, E. Farnea, S. M. Lenzi, S. Lunardi, A. Dewald, Th. Pissulla, S. Szilner, R. Broda, F. Recchia, A. Algora, L. Angus, D. Bazzacco, G. Benzoni, P. G. Bizzeti, A. M. Bizzeti-Sona, P. Boutachkov, L. Corradi, F. Crespi, G. de Angelis, E. Fioretto, A. Görgen, M. Gorska, A. Gottardo, E. Grodner, B. Guiot, A. Howard, W. Królas, S. Leoni, P. Mason, R. Menegazzo, D. Montanari, G. Montagnoli, D. R. Napoli, A. Obertelli, T. Pawłat, G. Pollarolo, B. Rubio, E. Şahin, F. Scarlassara, R. Silvestri, A. M. Stefanini, J. F. Smith, D. Steppenbeck, C. A. Ur, P. T. Wady, J. Wrzesiński, E. Maglione, and I. Hamamoto, "Lifetime measurements of the neutron-rich $n = 30$ isotones ^{50}Ca and ^{51}Sc: Orbital dependence of effective charges in the fp shell," Phys. Rev. Lett. **102**, 242502 (2009).

[43] R. du Rietz, J. Ekman, D. Rudolph, C. Fahlander, A. Dewald, O. Möller, B. Saha, M. Axiotis, M. A. Bentley, C. Chandler, G. de Angelis, F. Della Vedova, A. Gadea, G. Hammond, S. M. Lenzi, N. Mărginean, D. R. Napoli, M. Nespolo, C. Rusu, and D. Tonev, "Effective Charges in the fp Shell," Phys. Rev. Lett. **93**, 222501 (2004).

[44] A. Poves, F. Nowacki, and E. Caurier, "Isovector effective charge and the staggering of $2^+ \to 0^+$ transition probabilities in the titanium isotopes," Phys. Rev. C **72**, 047302 (2005).

[45] B. A. Brown, A. Arima, and J. B. McGrory, "E2 core-polarization charge for nuclei near ^{16}O and ^{40}Ca," Nuclear Physics A **277**, 77–108 (1977).

[46] S. Raman, C. W. Nestor, and P. Tikkanen, "Transition Probability from the ground to the First-excited 2^+ state of even-even Nuclides," Atomic Data and Nuclear Data Tables **78**, 1 – 128 (2001).